Reduced Ion Crossover in Bipolar Membrane Electrolysis via Increased Current Density, Molecular Size, and Valence

Blommaert, Marijn A.; Verdonk, Joost A.H.; Blommaert, Hester C.B.; Smith, Wilson A.; Vermaas, David A.

DOI
10.1021/acsaem.0c00687

Publication date
2020

Document Version
Final published version

Published in
ACS Applied Energy Materials

ACS APPLIED ENERGY MATERIALS

www.acsaem.org

Article

Reduced Ion Crossover in Bipolar Membrane Electrolysis *via* Increased Current Density, Molecular Size, and Valence

Marijn A. Blommaert, Joost A. H. Verdonk, Hester C.B. Blommaert, Wilson A. Smith, and David A. Vermaas*

Cite This: *ACS Appl. Energy Mater.* 2020, 3, 5804−5812

Read Online

ACCESS | Metrics & More | Article Recommendations | Supporting Information

ABSTRACT: A bipolar membrane (BPM) can be used to accelerate water dissociation to maintain a pH gradient in electrochemical cells, providing freedom to independently optimize the environments and catalysts used for paired reduction and oxidation reactions. The two physical layers in a BPM, respectively, selective for the exchange of cations and anions, should ideally reject ion crossover and facilitate ionic current *via* water dissociation in an interfacial layer. However, ions from the electrolyte do cross over in actual BPMs, competing with the water dissociation reaction and negatively affecting the stability of the electrolytes. Here, we explore the mechanisms of ion crossover as a function of pH and current density across a commercial BPM. Our unique series of experiments quantifies the ion crossover for more than 10 electrolyte combinations that cover 10 orders of magnitude in acid dissociation constant (K_a) and current densities spanning over more than 2 orders of magnitude. It was found that the ion crossover is dominated by diffusion for current densities up to a maximum of 10−40 mA cm^{-2} depending on the electrolyte, while migration is of higher importance at high current densities. The influence of the electrolyte pK_a or pH on the ion crossover is not straightforward. However, ions with a higher valence or ion size show significantly lower crossover. Moreover, high current densities are the most favorable for high water dissociation efficiencies for all electrolyte combinations. This operational mode aligns well with practical applications of BPMs in electrolysis at industrial relevant current densities.

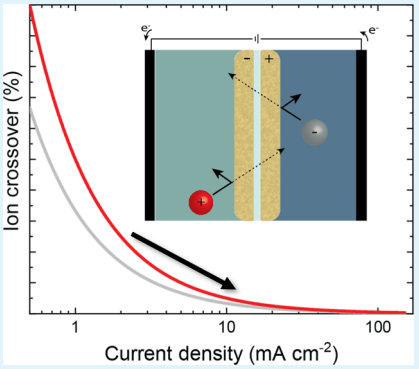

KEYWORDS: *bipolar membranes, ion crossover, ion transport, electrochemistry, pK_a, valence, current density*

INTRODUCTION

Research and adoption of new renewable energy technologies is accelerated by the combined rapidly decreasing costs of solar- and wind-derived electricity and increasing governmental requirements to limit CO_2 emissions. The renewable energy capacity is expected to reach 5 TW by 2030,[1] which exceeds the average electricity consumption of 3.5 TW.[2] However, renewables deal with a strongly fluctuating production, expressed by the utilization factor of approximately 20%.[3] Thus, long-term energy storage in the form of synthetic fuels is indispensable to cope with the intermittency (daily and seasonally) of the renewable electricity sources.[4] Such fuels can be produced *via* electrochemical technologies, which have the potential to directly convert (renewable) electrical energy to chemical bonds. Examples include the water-splitting reaction and electrocatalytic reduction of carbon dioxide (CO_2RR), producing hydrogen and various carbon products, respectively.[5] To make these systems perform efficiently at scales relevant for the global energy supply,[6] these reactions should be performed at high current density, high energy efficiency, and with Earth-abundant materials. These constraints require minimizing the applied potential for the entire electrochemical cell, including losses associated with overpotentials for the combined oxidation and reduction reactions, the electrolyte resistance, and membrane functionality.

Considering that the optimal conditions of electrolytes for given redox reactions often differ from each other, a bipolar membrane (BPM) can be implemented to maintain optimized conditions for both half-reactions.[7−12] A BPM consists of a cation and anion exchange layer (CEL and AEL), which are connected by an interfacial layer (IL). This configuration efficiently impedes charged species in the surrounding electrolytes from being transported through the BPM.[13] To maintain the ionic transport within the overall electrochemical cell, the water dissociation reaction (WDR) occurs at the interfacial layer between the CEL and AEL.[14,15] The WDR, which can be enhanced by the deposition of catalysts[16−19] at the interfacial layer, generates protons and hydroxide ions in the IL at an accelerated rate compared to the water dissociation rate in water.

Received: April 3, 2020
Accepted: May 27, 2020
Published: May 27, 2020

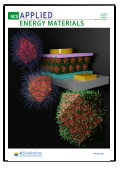

When a reverse bias is applied (*i.e.*, when the CEL faces the cathode), the protons and hydroxide ions are removed from the IL through the CEL and AEL, respectively, which keeps the WDR to proceed.[20−22]

In reality, products of the WDR (H^+ and OH^-) are not the only ions present in the interfacial layer. First, electrolyte salt ions with a charge opposite of the fixed charge of the adjacent membrane layer (*i.e.*, counter ions) can enter the first membrane layer through diffusion. Second, a minority of salt ions with the same charge (*i.e.*, co-ions) can enter the membrane layer because of the finite charge density of the polymer structure, as described in the Teorell−Meyer−Sievers theory,[23,24] and subsequently reach the interfacial layer. Dependent on the concentration and potential gradient across the membrane, these species can slowly diffuse and/or migrate in a process called ion crossover. When this ion is migrating, the WDR efficiency is reduced because the charge carried by ion crossover cannot be used to release protons and hydroxide ions from the IL. For a water electrolysis cell, where protons are being consumed at the cathode and hydroxides at the anode, ion crossover gradually destabilizes the electrolyte pH values and causes mixing of the two electrolytes.[25] Hence, ion crossover should be minimized in order to maintain optimal and stable conditions at the electrodes and avoid electrolyte regeneration or catalyst degradation.

Very little literature discusses the impact of ion crossover through a BPM. Experimental work is limited to a small set of electrolytes and current densities, which is insufficient to understand how ion crossover can be effectively minimized in practical applications because of the wide variety of experimental conditions and materials. Moussaoui *et al.* showed that higher current densities and lower salt concentrations generally decrease the relative ion crossover.[25] The effect of current density was confirmed by Sun *et al.*,[26] while Vermaas *et al.* showed that some common ions with larger hydrated radii demonstrate a lower ion crossover.[20] The latter also established a link between the pH and current−voltage (i−V) curves of a BPM. However, each previous crossover work was performed at a single pH all different from each other and using different electrolytes and a different range in current density. At the same time, it is likely that the pH is of major importance for ion crossover, as the molar fractions of ions, protons, and hydroxides in the membrane determine the ion migration and WDR. Also, the ion valence and pK_a of the electrolyte ions are expected to impact the concentration in the membrane moiety and thus its crossover. A good understanding of the electrolyte properties on ion crossover is additionally motivated by the significant effect of electrolytes on the efficiency and selectivity of the reduction and oxidation reactions at the anode and cathode.[27] For example, it is established that bigger cations suppress the hydrogen evolution reaction (HER) and promote CO_2RR.[28] Hence, the choice of the electrolytes is crucial for the performance of the entire electrochemical cell, and therefore, the electrolyte-dependent ion crossover is needed to be further understood to enable highly efficient electrochemical systems. However, none of the previous work systematically investigated the impact of pK_a and pH on ion crossover, let alone in combination with current density, concentration, and ionic radius. In this work, we focus on ion crossover through a BPM, using 10 different catholytes in four distinct pK_a regimes and tested at various current densities. The different catholyte properties allow the ability to experimentally observe the effect of pH and ion size on ion crossover, providing a useful guide for a proper electrolyte choice.

THEORY

Mass transport of ions in a BPM exists because of a gradient in electrochemical potential $\bar{\mu}$.[29] This electrochemical potential gradient arises from two components: a concentration gradient driving diffusion and an electric field gradient driving ion migration. Convective transport in the membrane is neglected because of the nonporous structure of a membrane.[30] The mass transport, described by the flux J_k of ions k, is given by the Nernst−Planck (NP) equation[29]

$$J_k = -\frac{C_k D_k}{RT}\frac{\partial \bar{\mu}}{\partial x} = -D_k\frac{\partial C_k}{\partial x} - \frac{z_k F}{RT}C_k D_k\frac{\partial \varphi}{\partial x} \quad (1)$$

where C_k is the concentration of species k with a valence z_k, D_k is the diffusion coefficient, F is the Faraday constant, R is the gas constant, and T is the temperature. The directions of diffusion and migration for several ionic species in an electrochemical cell are schematically represented in Figure 1. It is important to note

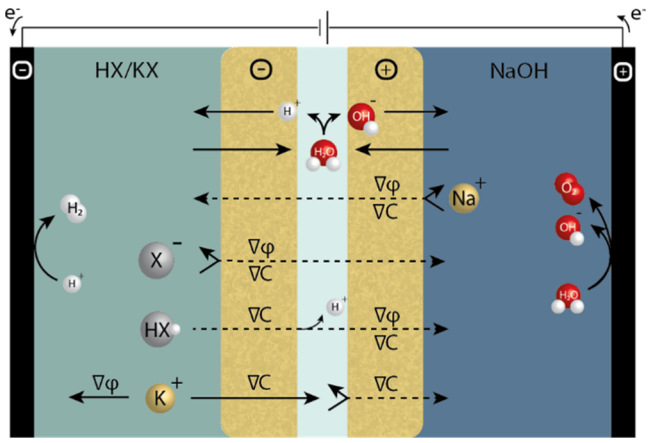

Figure 1. Schematic representation of an electrochemical cell with the WDR and different ion transport mechanisms described in a BPM. Ion transport that is not impeded by fixed charges (such as the WDR on top) is described by a solid line; ion crossover is represented by a dotted line.

that diffusion of an ion can never occur alone to comply with electroneutrality. To maintain electroneutrality, it should be either neutralized by an ion of the opposing charge travelling in the same direction, or from the same charge in the opposite direction, or maintained by consumed ions in the reaction. In the latter case, the anolyte will turn more acidic and the catholyte will turn more alkaline. Hence, the chemical potential difference between the two compartments is reduced, requiring a higher electrical potential to compensate. Also, assuming initial conditions with a more alkaline anolyte compared to the catholyte, the ionic strength is reduced when ion crossover is balanced by redox reactions that create H^+ neutralizing the alkaline anolyte or OH^- neutralizing the acidic catholyte. Altogether, ion crossover should be minimized to sustain a favorable environment for the electrolysis reactions.

Equation 1 suggests that the electrolyte properties, such as ion charge (z_k) and diffusion coefficient (D_k), influence the ion crossover. However, as the diffusion coefficient and local concentration inside the two membrane layers are unknown,[31,32] there is insufficient data to accurately simulate the ion crossover in this region. Moreover, the membrane fixed charge density and degree of cross-linking affect the selectivity toward ions of different valences or sizes.[13,33] The multitude of

https://dx.doi.org/10.1021/acsaem.0c00687
ACS Appl. Energy Mater. 2020, 3, 5804−5812

Table 1. Summary of Tested Catholytes and Anolytes with Their Chemical Formula, pK_a, Molecular Weight (M_W), pH at the Start of the Measurement, Products (HBr or KOH) Added to Achieve a pH Equivalent to Its Acid Dissociation Constant (pK_a), and Conductivity of Solution (σ)[a]

catholyte	chemical formula	pK_a	M_W (g mol^{-1})	pH$_{solution}$	addition	σ (mS cm^{-1})
tricine	$C_6H_{13}NO_5$	2.023	179.17	1.99	0.28 M HBr	20.7
phosphate	H_3PO_4/KH_2PO_4	2.148	98.00	2.03		26.0
glycine	$C_2H_5NO_2$	2.351	75.07	2.35	0.16 M HBr	25.3
MOPS	$C_7H_{15}NO_4S$	7.184	209.26	7.18	0.18 M KOH	11.5
BES	$C_6H_{15}NO_5S$	7.187	213.25	7.12	0.21 M KOH	14.7
phosphate	KH_2PO_4/K_2HPO_4	7.198	96.99	6.74		51.0
AMPSO	$C_7H_{15}NO_5S$	9.138	227.28	9.14	0.34 M KOH	13.0
boric acid	H_3BO_3	9.237	61.83	9.19	0.21 M KOH	16.5
potassium bicarbonate	$KHCO_3$	10.329	61.02	10.33	0.34 M KOH	70.8
CAPS	$C_9H_{19}NO_3S$	10.499	221.32	10.44	0.37 M KOH	10.8
anolyte	chemical formula	pK_a	M_W (g mol^{-1})	pH$_{solution}$	addition	σ (mS cm^{-1})
sodium hydroxide	NaOH		40.00	13.30		100.0

[a]All catholytes had a concentration of 0.5 M total of acid and base species.

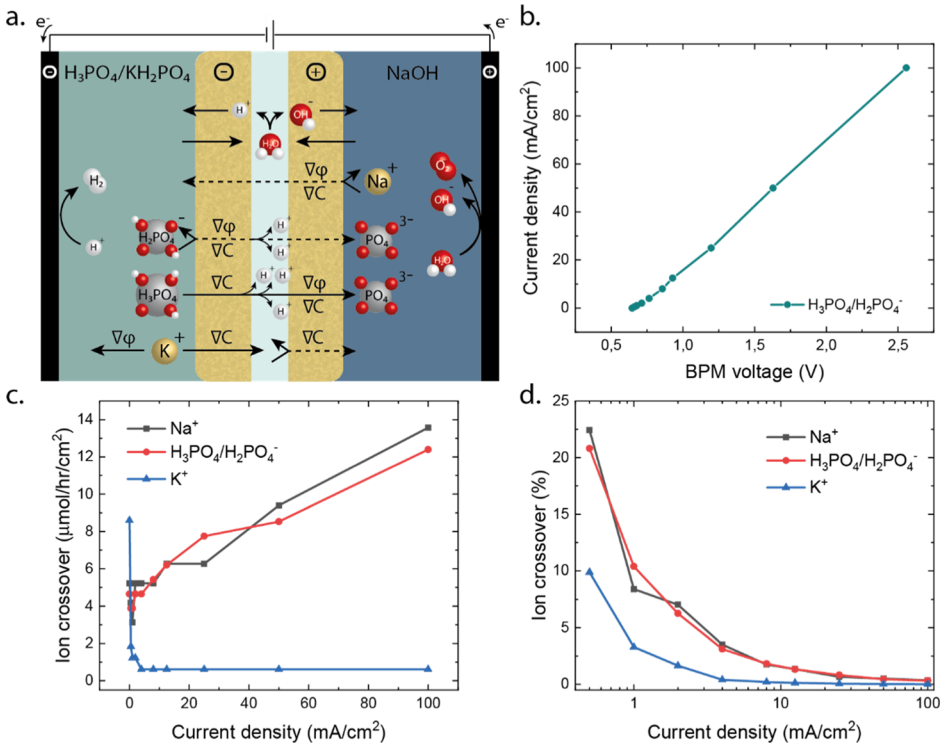

Figure 2. (a) Schematic illustration of ion-transport mechanisms for a phosphate buffer (0.25 M H_3PO_4 + 0.25 M $KHPO_4$) as a catholyte and 0.5 M NaOH as an anolyte, with (b) iR-corrected $i-V$ curve of the membrane response among these electrolytes. The ion crossover of the ions present in these electrolytes is shown in (c) absolute numbers. and (d) relative crossover of the total charge as a function of current density in a linear and logarithmic scale, respectively. For improved readability, a representative data set is selected.

electrolytes and membrane parameters that impact the ion concentration and potential in the membrane (eq 1) requires more experimental exploration to understand and control ion crossover in BPMs.

METHODS

Membrane Cell. A commercially available BPM (Fumatech Fumasep BPM) was used to perform electrochemical experiments. Membrane characteristics are given in Table S2. A MicroFlowCell (ElectroCell) flow cell was used (see Figure S4), with a surface area of 10 cm^2 and with a Pt-coated cathode and anode. A constant current density was applied for 45 min. The applied current densities were varied from 0 to 150 mA cm^{-2}. The current densities were applied in a random order to avoid a misleading relation between ion crossover and aging. By keeping the duration of the experiment fixed, the ion crossover by diffusion should remain equal for all experiments. The voltage across the BPM was measured with two microreference electrodes at a distance of 2.14 mm from the membrane surfaces and was iR-corrected based on the measured conductivities of the electrolytes used. The electrolyte was pumped through the respective cathode and anode compartments with a constant flow rate of 0.07 mL s^{-1}.

Electrolytes. Four pK_a groups were selected to determine the pH dependency. Each pK_a group contains different electrolytes with a similar pK_a,[34] which excludes the pH effect in the group itself. Within a pK_a group, electrolytes were selected with a significant difference in ion size, represented by the molecular weight, as the Stokes radius used in previous work[20] was not available for many organic catholytes used here. These organic electrolytes also require an addition of either an

https://dx.doi.org/10.1021/acsaem.0c00687
ACS Appl. Energy Mater. 2020, 3, 5804−5812

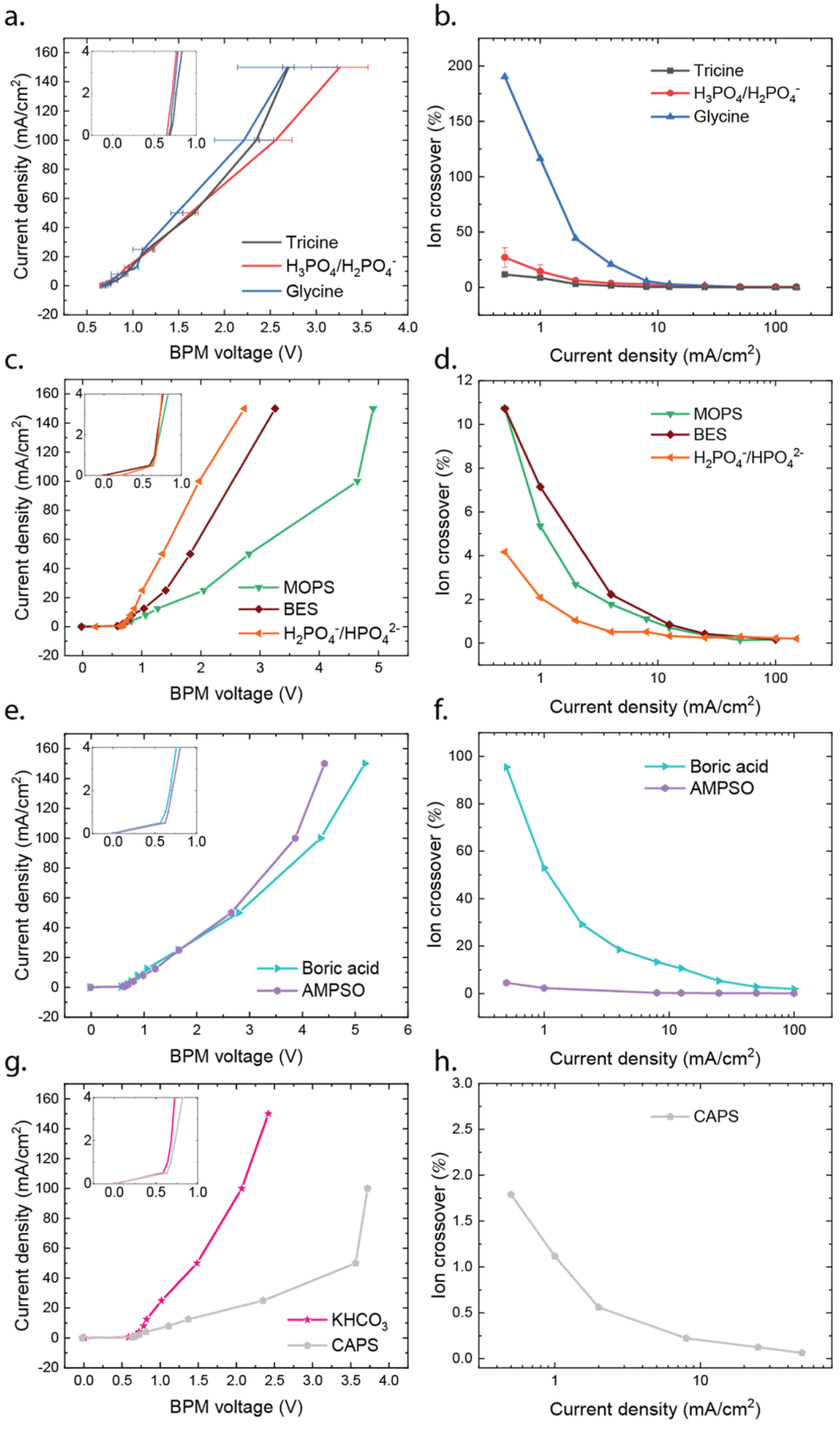

Figure 3. $i-V$ curve and relative ion crossover of the catholyte ions, for (a,b) pK_a 2 group with data from an average of three measurement runs for reproducibility purposes where the error bars indicate the calculated mean square error, (c,d) pK_a 7 group, (e,f) pK_a 9 group, and (g,h) pK_a 10 group. For the $KHCO_3$ buffer, no ion crossover data of (bi)carbonate were obtained. Absolute ion crossover data are presented in Figure S1.

acid (HBr) or base (KOH) to reach the pH of their respective pK_a. All electrolytes had an equimolar concentration of 0.5 M of an acid/base and conjugate base/acid, according to the following reaction $HX \rightleftharpoons H^+ + X^-$, where X is the respective buffer species.

Between every experiment, the cell was thoroughly cleaned and a new membrane was used. After every experiment, a sample was taken of the electrolytes, and ion crossover was analyzed with an ion-coupled plasma optical emission spectrometer. Because glycine and tricine have

https://dx.doi.org/10.1021/acsaem.0c00687
ACS Appl. Energy Mater. 2020, 3, 5804−5812

no elements detectable by ion-coupled plasma optical emission spectrometry (ICP-OES), their ion crossover was analyzed with nuclear magnetic resonance (NMR). More specifications on the cell and chemicals used can be found in the Supporting Information.

All electrolytes were considered to have an average valence of one for determining the relative ion crossover. Because the conditions at the anolyte were the same for each experiment, a statistical analysis was performed on the Na^+ crossover.

RESULTS

Ten different catholytes were paired with 0.5 M NaOH as the anolyte across the BPM. To assess the pH dependency, four groups of catholyte buffers were chosen with a distinctive pK_a (2, 7, 9, and 10). All tested catholytes and anolytes, with their respective parameters, are summarized in Table 1. As a reference case, we first discuss the crossover of phosphate buffer (H_3PO_4/KH_2PO_4) *versus* NaOH across a BPM at various current densities.

Reference Case: the Phosphate Buffer (pH2). Figure 2a illustrates the possible transport mechanisms for the ionic species in these electrolytes across a BPM when a current is applied to the phosphate buffer (pH2) *versus* NaOH electrolyte case. The $i-V$ curve for the BPM is plotted in Figure 2b. The absolute ion crossover of species from the phosphate buffer (H_3PO_4, $H_2PO_4^-$, and K^+) and Na^+ from the anolyte is given in Figure 2c. When this ion crossover flux is compared as a function of the total molar charge flux ($J = i/F$) with i (mA cm^{-2}) the current density that is applied, a relative ion crossover is obtained, which is shown in Figure 2d. The sum of all exchanged ions can be added up to estimate the total ion crossover as a function of applied current density. The remaining part of the charge is attributed to the WDR and is therefore a measure for the efficiency of the WDR.

Figure 2c shows that the crossover of ions, which are transported by diffusion and migration, and the total crossover of $H_2PO_4^-$ and Na^+ increase with increasing current density. The diffusional component, derived from a zero current density when migration is absent, is around 4 μmol h^{-1} cm^{-2} for both ions. According to the NP equation, the transport *via* migration should be proportional to the potential gradient across the BPM. Because the BPM voltage and current density are nearly linearly related in our experiments (Figure 2b), the NP equation also predicts a linear trend of the ion crossover as a function of current density. This is in agreement with our measurement in Figure 2c, which shows a linear slope of 0.08 μmol h^{-1} mA^{-1} for $H_2PO_4^-$ and 0.09 μmol h^{-1} mA^{-1} for Na^+.

The linear relation between crossover and current density also provides information on the phosphate crossover mechanism. At pH 2, phosphate can either cross over as $H_2PO_4^-$ or as H_3PO_4. In the latter, the uncharged H_3PO_4 species diffuses through the CEL. When $H_2PO_4^-$ or H_3PO_4 reach the membrane interface layer, the conditions change rapidly from acidic to alkaline. It is hypothesized that protons are liberated from H_3PO_4 and $H_2PO_4^-$ and will be consumed in the interaction with the WDR or surrounding OH^- (Figure 2a). The net effect of this crossover is a deficit of OH^- in the anolyte compared to the unaffected WDR, while this mechanism does not change the catholyte pH. Because the phosphate crossover shows a linear dependency on current density and because H_3PO_4 diffusion is not dependent on the current density, the crossover mechanism at high current goes either *via* $H_2PO_4^-$, or the diffusion of H_3PO_4 in the CEL is not rate-limiting. This will be further assessed when comparing it to other species (see effect of ion valence).

For all species, the relative crossover decreases with increased current density (Figure 2d). Based on the Faraday constant, a total (monovalent) charge equivalent of 37 μmol cm^{-2} h^{-1} mA^{-1} is transported. That means, for high current densities, when diffusion is negligible, $H_2PO_4^-$ and Na^+ crossovers are both responsible for 0.3% of the charge transport. Hence, the relative crossover decreases asymptotically to this value for $H_2PO_4^-$ and Na^+, as shown in Figure 2d, when increasing the current densities. This demonstrates that the WDR becomes the main driver of ion transport at medium to high current densities. Current densities of 5 mA/cm^2 and higher imply that more than 95% of the charges are being carried by protons and hydroxide ions from the WDR.

Given the absolute ion crossover of K^+ of 9 μmol h^{-1} cm^{-2} at 0 mA cm^{-2}, the diffusion of K^+ is larger than that of Na^+ and phosphate (Figure 2c). As the conditions at 0 mA cm^{-2} do not allow net charge transport over the BPM, the flux of K^+ is compensated by Na^+ crossover in the opposite direction or cotransport with $H_2PO_4^-$. This is in agreement with the K^+ crossover at zero current being approximately equal to the sum of Na^+ and phosphate crossover. When a small current (0.5 mA cm^{-2}) is applied, the K^+ crossover already drops to 2 μmol h^{-1} cm^{-2}. The downward trend at higher current densities continues in both absolute and relative terms, indicating that migration indeed reverts the potassium transport instead of driving it through the BPM, as hypothesized in Figure 2a. As a result, also the relative potassium crossover reduces asymptotically to near 0% for high current densities (Figure 2d).

Probing the Effect of pK_a on Ion Crossover. To compare the ion crossover of different electrolytes with the same pH and buffering strength, the relative ion crossover of all 10 catholytes is presented in Figure 3b,d,f,h, grouped by pK_a. In addition, the respective $i-V$ curves across the BPMs are shown in Figure 3a,c,e,g.

The majority of the $i-V$ curves demonstrate a plateau at current densities <0.5 mA cm^{-2}, while for the pK_a 2 group, a plateau at positive currents is absent as expected from the significant pH difference (ΔpH > 11).[20] These results differ from the earlier reported plateau current densities, which were measured with galvanodynamic scans and in a flow cell with a larger shear velocity.[16] The crossover in all pK_a groups shows a decrease in relative ion transport when the current density is increased, in agreement with previous findings.[25,26] This extensive dataset shows a linear regression for absolute ion crossover in nearly all electrolytes ($y_{ioncrossover} = \alpha_{diff} + \beta_{migr} \cdot j$), as shown in Table S1. Diffusion is responsible for the majority of the ion crossover under a current density that varies from 10 to 40 mA cm^{-2} depending on the electrolyte (Figure S1). When a neutral conjugate is present (*e.g.*, H_3PO_4), transport by diffusion increases.

Nevertheless, Figure 3 also demonstrates large differences in crossover magnitude between the ions, with extremely high crossover for boric acid and glycine. Because the crossover of these ions deviates from other electrolytes with similar pK_a and pH, we have further studied possible differentiating factors in ionic properties.

Effect of Ion Valence. The effect of ion valence on their crossover rate across a BPM can be demonstrated using a phosphate buffer at pH 2 and pH 7. However, the ion crossover of the phosphate buffer at pH 7 also has barely any crossover at 0 mA cm^{-2}, while the equimolar phosphate buffer at pH 2 has a

https://dx.doi.org/10.1021/acsaem.0c00687
ACS Appl. Energy Mater. 2020, 3, 5804−5812

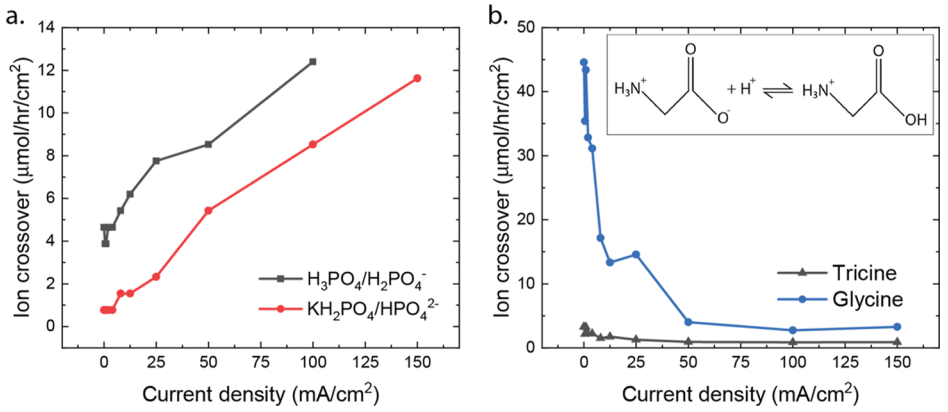

Figure 4. Absolute ion crossover of the (a) phosphate buffers at pK_a 2 (black) and pK_a 7 (red), which illustrate the dependence of valence for ion crossover and (b) glycine and tricine buffers with cationic species, with the equilibrium reaction of glycine under acidic conditions in the inset. The tricine structure has the same backbone as glycine, with a tris(hydroxymethyl)methyl group attached.

crossover rate of 4 μmol h^{-1} cm^{-2} at 0 mA cm^{-2} (Figure 4a). This can be explained by the neutral species, H_3PO_4, which is only diffusion-driven and adds a constant amount of crossover compared to the buffer at pH 7 throughout all current densities. The absence of uncharged species and a higher (average) ion charge at pH 7 causes stronger repelling of ions by the fixed charges of the CEL. From a practical point of view, there are multiple advantages of using a higher valence phosphate, as multivalent species provide higher concentration of K^+ and therefore result in a higher conductivity (Table 1), lowering the resistance losses of the electrolytes. As the current density increases, the phosphate crossover due to migration increases linearly, with similar slopes at both pH 2 and pH 7. This suggests that $H_2PO_4^-$ is responsible for the crossover at high current densities rather than the earlier mentioned mechanism *via* H_3PO_4 and its deprotonation at the BPM interface (Figure 2).

Similarly, glycine and boric acid, which have neutral species, show a high ion crossover because of diffusion at 0 mA cm^{-2} (Figure 3). In specific, glycine has a zwitter-ionic nature: $H_2A^+ \leftrightarrow HA$, without a negatively charged component, as schematically shown in the inset of Figure 4b. The tricine buffer is comparable to glycine in the pK_a 2 group, also having neutral and cationic species but has a larger molecular weight. For both glycine and tricine ions, migration transports the cations away from the BPM, which is visible in the downward trend of the absolute ion crossover, see Figure 4b. However, the ion crossover of tricine is an order of magnitude lower than that of glycine. As tricine has a much larger ionic radius, the effect of the ionic radius for all ions is being further assessed.

Effect of Ionic Size. The dependency of ion size, expressed in molecular weight, on the ion crossover is illustrated in Figure 5 for all sets of electrolyte pairs. It can be seen that the ion crossover decreases with increasing molecular weight. Especially boric acid has a low ionic radius, explaining the high ion crossover. As membranes have limited interstitial spaces, ions with a molecular weight of 100 g mol^{-1} and higher are subject to strong steric hindrance and show minimal crossover.

Although these results imply that larger molecules may be advantageous for use in stable electrochemical systems, the higher molecular weights typically also feature a lower conductivity and solubility than smaller ionic species. This effect may lead to extra resistive losses in the electrolyte as well as in the membrane layer itself. The latter is visible in Figure 3c,e,g

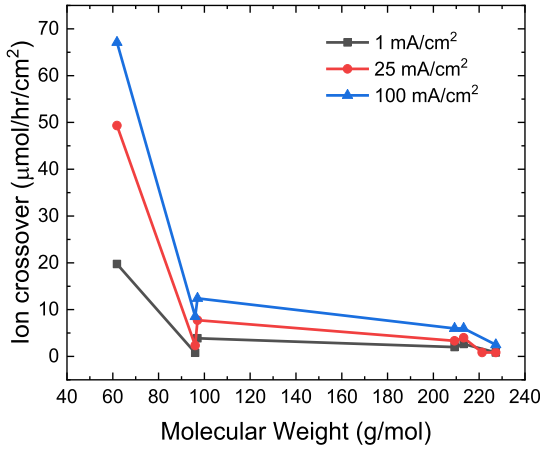

Figure 5. Ion crossover of catholytic anions as a function of molecular weight. Glycine and tricine are excluded because of their zwitterionic form, and no anion crossover of $KHCO_3$ is measured. Figure S2b represents the same data without boric acid (M_W 61.8 g mol^{-1}), which still shows a decreasing trend.

where the larger molecules show an increased membrane voltage, similar to monopolar membranes.[35]

Na^+ Crossover. Although anions are transported by migration from the catholyte to anolyte, the electric field forces cations from the anolyte to the catholyte when a reverse bias is applied. Because the NaOH anolyte is used as a constant factor in all experiments in this study, the effect of the opposing electrolyte on the Na^+ ion crossover can be isolated. According to the NP equation (see eq 1), the electric potential gradient and Na^+ properties should determine the migration of Na^+, suggesting a linear relation with the membrane voltage independent of the opposing electrolyte.

Indeed, a linear trend for all electrolyte pairs as predicted from eq 1 is shown in Figure 6a. The gap of data between 0 and 0.8 V reflects the plateau current density and explains the large collection of data points just above 0.8 V because of an intensification of measurements at low current densities. For each electrolyte combination, a simple linear regression is calculated to predict the ion crossover of Na^+ through a BPM based on the membrane voltage (Figure 6a, Table S1). All fits have an intercept reasonably close to the origin, which indicates that the Na^+ crossover is mainly driven by migration. Most slopes are similar, while the i–V curves show much more

https://dx.doi.org/10.1021/acsaem.0c00687
ACS Appl. Energy Mater. 2020, 3, 5804−5812

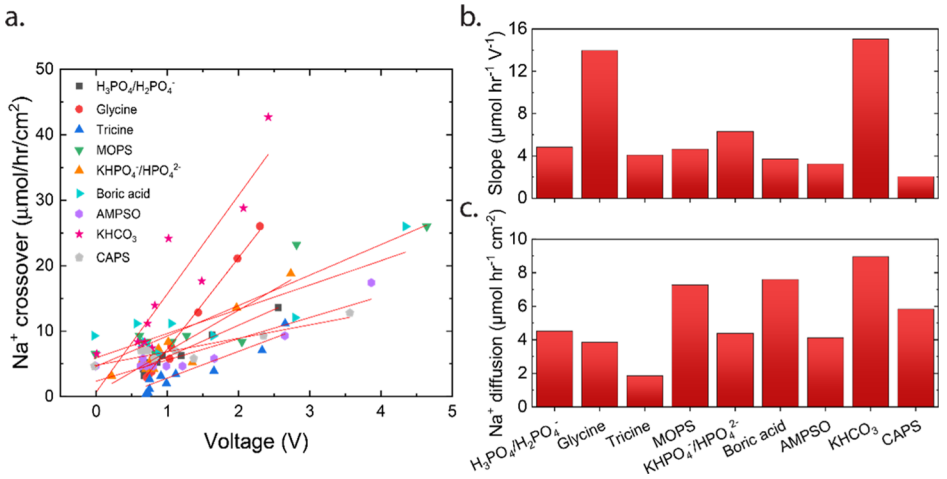

Figure 6. (a) Ion crossover of Na^+ through a BPM opposing different buffers as a function of the BPM voltage, (b) slope of the Na^+ crossover in function of membrane voltage for each opposing electrolyte, and (c) Na^+ diffusion rates for each opposing electrolyte. The corresponding linear regression equations and R^2 values are provided in Supporting Information (Table S1).

variation, which justifies the use of voltage as the determining factor for ion crossover. However, when bicarbonate and glycine are used as the catholyte, the crossover of Na^+ increases more dramatically with increasing voltage (Figure 6b). It is important to note that the crossover of glycine reduces with increasing current density (Figure 3b), while that of Na^+ crossover increases steeply with increasing voltage and current.

The dependency of the opposing electrolyte composition on the Na^+ crossover is surprising, as the anion exchange membrane is the first and only electronically repelling layer for Na^+. Although the membrane−membrane interface should in theory be of no influence for the crossover of the sodium ions, Figure 6a demonstrates that the crossover of the separated electrolytes is still dependent on one another. More specifically, the diffusion rate for Na^+ can be found *via* the *y*-intercept of the corresponding linear regression equations based on the current density and show a similar dependence on the opposing electrolyte (Figure 6c). One could speculate that glycine and (bi)carbonate shield off fixed charges in the AEL, which would facilitate the Na^+ crossover. However, the ion valence of glycine and (bi)carbonate is not uniquely compared to the other tested electrolytes, which cannot justify this hypothesis directly. Also, this dependency does not relate to the MW of the opposing electrolyte (Figure S2a). Although the absolute Na^+ crossover may vary with membrane production batches, demonstrated by a 4 times higher crossover when membranes from different batches are used (see Supporting Information, Figure S3), the same dependency on the opposing electrolytes is consistent throughout membrane batches. A similar trend is visible for a given electrolyte, as well as the trend among different electrolytes, showing the significance of our results independent of the batch used. The pH (or pK_a) and ion size of the opposing electrolytes do neither provide an explanation. Thus, a clear justification is not readily available from the investigated parameters, and further investigation is required to understand the difference in crossover of the Na^+ as a function of the opposing electrolyte across a BPM.

CONCLUSIONS

Ion crossover negatively affects the stability of both electrolytes in energy technologies and is affected by voltage, ion size, valence, pK_a, and charge density. The ion crossover in BPMs does follow the NP equation, reflected in a diffusion-driven crossover flux at zero current and a linearly increasing crossover rate because of migration. For all the studied cases, no limiting co-ion fluxes are reached, in contrast to earlier reported work.[28] At low current densities, depending on the electrolyte up to 10−40 mA cm^{-2}, diffusion accounts for the majority of the ion crossover, while at high current densities, migration is of higher importance. When relative ion crossover is considered, which is a measure for the stability of the electrolytes, the lowest relative crossover is obtained at high current density independent of any electrolyte combination, which favors the use of a BPM at high current density rates as in industrial applications. The selection of electrolytes involves a trade-off between low crossover (for larger ions) which usually comes at the expense of lower conductivity. The influence of the pK_a or pH of the catholyte does not have a straightforward influence on the ion crossover. However, the distinct difference in ion crossover of phosphate depending on the pH (pH 2 and 7) shows that a BPM is clearly better repelling ions with a higher average valence. The demonstrated effects of pH, ion size, current density, and membrane properties on the ion crossover can further guide the practical application of electrolytes and BPM development for electrochemical conversion.

ASSOCIATED CONTENT

Supporting Information

The Supporting Information is available free of charge at https://pubs.acs.org/doi/10.1021/acsaem.0c00687.

Absolute ion crossover, results of linear regression applied to ion crossover data, Na^+ crossover as a function of molecular weight of ions, data on membrane characteristics, and additional details on materials in the experimental setup (PDF)

AUTHOR INFORMATION

Corresponding Author

David A. Vermaas − *Department of Chemical Engineering, Delft University of Technology, 2629 HZ Delft, The Netherlands;* orcid.org/0000-0002-4705-6453; Email: d.a.vermaas@tudelft.nl

https://dx.doi.org/10.1021/acsaem.0c00687
ACS Appl. Energy Mater. 2020, 3, 5804−5812

Authors

Marijn A. Blommaert − *Department of Chemical Engineering, Delft University of Technology, 2629 HZ Delft, The Netherlands;* orcid.org/0000-0003-1568-0961

Joost A. H. Verdonk − *Department of Chemical Engineering, Delft University of Technology, 2629 HZ Delft, The Netherlands*

Hester C.B. Blommaert − *Department of Earth and Environmental Sciences, KU Leuven, 3001 Leuven, Belgium*

Wilson A. Smith − *Department of Chemical Engineering, Delft University of Technology, 2629 HZ Delft, The Netherlands;* orcid.org/0000-0001-7757-5281

Complete contact information is available at: https://pubs.acs.org/10.1021/acsaem.0c00687

Author Contributions

M.A.B., W.A.S., and D.A.V. wrote the manuscript with input from all co-authors. J.A.H.V. and M.A.B. performed the experiments and data analysis. H.C.B.B. performed statistical analysis.

Notes

The authors declare no competing financial interest.

■ ACKNOWLEDGMENTS

This research received funding from the Netherlands Organization for Scientific Research (NWO) under project number 733.000.008 in the framework of the Solar to Products programme co-funded by Shell Global Solutions International B.V. The authors would like to thank Baukje Terpstra for the ICP-OES measurements and Martin Kolen for performing the NMR measurements.

■ REFERENCES

(1) International Energy Agency. *Renewables 2018*, 2018.

(2) U.S. Energy Information Administration. *International Energy Outlook 2019*, 2020; vol. *2019*.

(3) Sinn, H.-W. Buffering volatility: A study on the limits of Germany's energy revolution. *Eur. Econ. Rev.* **2017**, *99*, 130−150.

(4) Smith, W. A.; Burdyny, T.; Vermaas, D. A.; Geerlings, H. Pathways to Industrial-Scale Fuel Out of Thin Air from CO2 Electrolysis. *Joule* **2019**, *3*, 1822−1834.

(5) Durst, J.; Rudnev, A.; Dutta, A.; Fu, Y.; Herranz, J.; Kaliginedi, V.; Kuzume, A.; Permyakova, A. A.; Paratcha, Y.; Broekmann, P.; Schmidt, T. J. Electrochemical CO2 Reduction − A Critical View on Fundamentals, Materials and Applications. *Chim. Int. J. Chem.* **2015**, *69*, 769−776.

(6) Burdyny, T.; Smith, W. A. CO2 reduction on gas-diffusion electrodes and why catalytic performance must be assessed at commercially-relevant conditions. *Energy Environ. Sci.* **2019**, *12*, 1442−1453.

(7) Luo, J.; Vermaas, D. A.; Bi, D.; Hagfeldt, A.; Smith, W. A.; Grätzel, M. Bipolar Membrane-Assisted Solar Water Splitting in Optimal pH. *Adv. Energy Mater.* **2016**, *6*, 1600100.

(8) Li, Y. C.; Zhou, D.; Yan, Z.; Gonçalves, R. H.; Salvatore, D. A.; Berlinguette, C. P.; Mallouk, T. E. Electrolysis of CO_2 to Syngas in Bipolar Membrane-Based Electrochemical Cells. *ACS Energy Lett.* **2016**, *1*, 1149−1153.

(9) Vermaas, D. A.; Sassenburg, M.; Smith, W. A. Photo-assisted water splitting with bipolar membrane induced pH gradients for practical solar fuel devices. *J. Mater. Chem. A* **2015**, *3*, 19556−19562.

(10) McDonald, M. B.; Ardo, S.; Lewis, N. S.; Freund, M. S. Use of bipolar membranes for maintaining steady-state pH gradients in membrane-supported, solar-driven water splitting. *ChemSusChem* **2014**, *7*, 3021−3027.

(11) Oener, S. Z.; Ardo, S.; Boettcher, S. W. Ionic Processes in Water Electrolysis: The Role of Ion-selective Membranes. *ACS Energy Lett.* **2017**, *2*, 2625.

(12) Lin, M.; Han, L.; Singh, M. R.; Xiang, C. An Experimental- And Simulation-Based Evaluation of the CO2 Utilization Efficiency of Aqueous-Based Electrochemical CO2 Reduction Reactors with Ion-Selective Membranes. *ACS Appl. Energy Mater.* **2019**, *2*, 5843−5850.

(13) Sata, T. *Ion Exchange Membranes : Preparation, Characterization, Modification and Application*; Royal Society of Chemistry, 2004.

(14) Simons, R.; Khanarian, G. Water dissociation in bipolar membranes: Experiments and theory. *J. Membr. Biol.* **1978**, *38*, 11−30.

(15) Strathmann, H.; Krol, J. J.; Rapp, H.-J.; Eigenberger, G. Limiting current density and water dissociation in bipolar membranes. *J. Membr. Sci.* **1997**, *125*, 123−142.

(16) McDonald, M. B.; Freund, M. S. Graphene oxide as a water dissociation catalyst in the bipolar membrane interfacial layer. *ACS Appl. Mater. Interfaces* **2014**, *6*, 13790−13797.

(17) Mel'nikov, S. S.; Shapovalova, O. V.; Shel'deshov, N. V.; Zabolotskii, V. I. Effect of d-metal hydroxides on water dissociation in bipolar membranes. *Pet. Chem.* **2011**, *51*, 577−584.

(18) Fu, R.; Xu, T.; Wang, G.; Yang, W.; Pan, Z. PEG-catalytic water splitting in the interface of a bipolar membrane. *J. Colloid Interface Sci.* **2003**, *263*, 386−390.

(19) Li, J.; Morthensen, S. T.; Zhu, J.; Yuan, S.; Wang, J.; Volodine, A.; Lin, J.; Shen, J.; Van der Bruggen, B. Exfoliated MoS 2 nanosheets loaded on bipolar exchange membranes interfaces as advanced catalysts for water dissociation. *Sep. Purif. Technol.* **2018**, *194*, 416−424.

(20) Vermaas, D. A.; Wiegman, S.; Nagaki, T.; Smith, W. A. Ion transport mechanisms in bipolar membranes for (photo)-electrochemical water splitting. *Sustainable Energy Fuels* **2018**, *2*, 2006−2015.

(21) Blommaert, M. A.; Vermaas, D. A.; Izelaar, B.; in 't Veen, B.; Smith, W. A. Electrochemical impedance spectroscopy as a performance indicator of water dissociation in bipolar membranes. *J. Mater. Chem. A* **2019**, *7*, 19060−19069.

(22) Ashrafi, A. M.; Gupta, N.; Neděla, D. An investigation through the validation of the electrochemical methods used for bipolar membranes characterization. *J. Membr. Sci.* **2017**, *544*, 195−207.

(23) Teorell, T. An Attempt to Formulate a Quantitative Theory of Membrane Permeability. *Proc. Soc. Exp. Biol. Med.* **1935**, *33*, 282−285.

(24) Meyer, K. H.; Sievers, J.-F. La perméabilité des membranes I. Théorie de la perméabilité ionique. *Helv. Chim. Chim Acta* **1936**, *19*, 649−664.

(25) Moussaoui, R. E.; Pourcelly, G.; Maeck, M.; Hurwitz, H. D.; Gavach, C. Co-ion leakage through bipolar membranes. Influence of I-V responses and water-splitting efficiency. *J. Membr. Sci.* **1994**, *90*, 283−292.

(26) Sun, K.; Liu, R.; Chen, Y.; Verlage, E.; Lewis, N. S.; Xiang, C. Solar-Driven Water Splitting: A Stabilized, Intrinsically Safe, 10% Efficient, Solar-Driven Water-Splitting Cell Incorporating Earth-Abundant Electrocatalysts with Steady-State pH Gradients and Product Separation Enabled by a Bipolar Membrane (Adv. Energy Mater. 13/2016). *Adv. Energy Mater.* **2016**, *6*, 1−7.

(27) Resasco, J.; Chen, L. D.; Clark, E.; Tsai, C.; Hahn, C.; Jaramillo, T. F.; Chan, K.; Bell, A. T. Promoter Effects of Alkali Metal Cations on the Electrochemical Reduction of Carbon Dioxide. *J. Am. Chem. Soc.* **2017**, *139*, 11277−11287.

(28) Resasco, J.; Lum, Y.; Clark, E.; Zeledon, J. Z.; Bell, A. T. Effects of Anion Identity and Concentration on Electrochemical Reduction of CO2. *ChemElectroChem* **2018**, *5*, 1064−1072.

(29) Bard, A. J.; Faulkner, L. R. *Electrochemical Methods Fundamentals and Applications*; Electrochemistry; Wiley, 1944.

(30) Krol, J. J. *Monopolar and Bipolar Ion Exchange Membranes*; Membrane Technology Group, 1997.

(31) Weng, L.-C.; Bell, A. T.; Weber, A. Z. Towards membrane-electrode assembly systems for CO2 reduction: A modeling study. *Energy Environ. Sci.* **2019**, *12*, 1950−1968.

(32) Mier, M.; Ibañez, R.; Ortiz, I. Influence of ion concentration on the kinetics of electrodialysis with bipolar membranes. *Sep. Purif. Technol.* **2008**, *59*, 197−205.
(33) Van der Bruggen, B. Membrane Technology. In *Kirk-Othmer Encyclopedia of Chemical Technology*; Wiley, 2017.
(34) Goldberg, R. N.; Kishore, N.; Lennen, R. M. Thermodynamic Quantities for the Ionization Reactions of Buffers. *J. Phys. Chem. Ref. Data* **2002**, *31*, 231−370.
(35) Luo, T.; Abdu, S.; Wessling, M. Selectivity of ion exchange membranes: A review. *J. Membr. Sci.* **2018**, *555*, 429−454.

https://dx.doi.org/10.1021/acsaem.0c00687
ACS Appl. Energy Mater. 2020, 3, 5804−5812